広島大学学術情報リポジトリ
Hiroshima University Institutional Repository

Title	High-Density Protein Loading on Hierarchically Porous LDH-Aluminum Hydroxide Composites with a Rational Mesostructure
Author(s)	Tokudome, Yasuaki; Fukui, Megu; Tarutani, Naoki; Nishimura, Sari; Prevot, Vanessa; Forano, Claude; Poologasundarampillai, Gowsihan; Lee, Peter D.; Takahashi, Masahide
Citation	Langmuir , 32 (35) : 8826 - 8833
Issue Date	2016-08-08
DOI	10.1021/acs.langmuir.6b01925
Self DOI	
URL	https://ir.lib.hiroshima-u.ac.jp/00053531
Right	© 2016 American Chemical Society This document is the Accepted Manuscript version of a Published Work that appeared in final form in Langmuir, copyright © American Chemical Society after peer review and technical editing by the publisher. To access the final edited and published work see https://doi.org/10.1021/acs.langmuir.6b01925 This is not the published version. Please cite only the published version. この論文は出版社版ではありません。引用の際には出版社版をご確認、ご利用ください。
Relation	

High-Density Protein Loading on Hierarchically Porous LDH-Aluminum Hydroxide Composites with a Rational Mesostructure

Yasuaki Tokudome,[*,a] *Megu Fukui,*[a] *Naoki Tarutani,*[a] *Sari Nishimura,*[a] *Vanessa Prevot,*[b,c] *Claude Forano,*[b,c] *Gowsihan Poologasundarampillai,*[d] *Peter D. Lee,*[d] *and Masahide Takahashi*[a]

[a] Department of Materials Science, Graduate School of Engineering, Osaka Prefecture University, Sakai, Osaka, 599-8531, Japan. [b]Université Clermont Auvergne Université Blaise Pascal, Institut de Chimie de Clermont-Ferrand, BP 10448, F-63000 Clermont-Ferrand, France. [c]CNRS, UMR 6296, ICCF, F-63171 Aubiere, France. [d] School of Materials, The University of Manchester, Oxford Rd., Manchester M13 9PL, UK.

Abstract

Hierarchically porous biocompatible Mg-Al-Cl type LDH composites containing aluminum hydroxide (Alhy) have been prepared using a phase-separation process. The sol-gel synthesis allows for the hierarchical pores of the LDH-Alhy composites to be tuned, leading to a high specific solid surface area per unit volume available for high molecular weight protein adsorptions. A linear relationship between effective surface area, S_{EFF}, and loading capacity of a model protein, bovine serum albumin (BSA) is established following successful control of the structure of the LDH-Alhy composite. The threshold of mean pore diameter, D_{pm}, above which BSA is effectively adsorbed on the surface of LDH-Alhy composites, is deduced as 20 nm. In particular, LDH-Alhy composite aerogels obtained via supercritical drying exhibits extremely high capacity for protein loading (996 mg/g) due to a large mean mesopore diameter (> 30 nm). The protein loading on LDH-Alhy is >14 times that of a reference LDH material (70 mg/g) prepared via a standard procedure. Importantly, BSA molecules pre-adsorbed on porous composites were successfully released on soaking in ionic solutions (HPO_4^{2-} and Cl^- aq.). The superior

capability of the biocompatible LDH materials for loading, encapsulation, and releasing large quantity of proteins was clearly demonstrated, which potential uses in separation and purification in addition to a high-capacity storage medium.

Introduction

Protein immobilization on solid surfaces is of relevance to a wide range of research areas with potential applications in biotechnology and physiology.[1] The activity of immobilized proteins is an important consideration which affects inorganic/bio interfacial properties, such as antifouling and antibacterial properties,[2] and hemo-/bio-compatibilities.[3] Various solids have been studied as supports for proteins,[1] including layered double hydroxides (LDHs), which are promising candidates due to their outstanding biocompatibility and an ability to limit denaturation of immobilized proteins.[4] The active conformation of proteins is retained on two-dimensionally flat and highly hydrophilic surfaces of LDHs,[5] to avoid denaturation which otherwise takes place on curved inorganic surfaces.[6-7] As a result, heme proteins, which usually denature on inorganic solids, can be immobilized on LDH surfaces without losing their inherent activity. Immobilized heme proteins are currently used as bio-electrodes with high sensitivity.[8-9]

Synthesizing LDHs with meso/macropores is highly promising to achieve high capacity loading of protein. The rational design of the porous structure in nm to sub-μm scale is especially important because micropores (< 2 nm) and relatively small mesopores, that typically adsorb ion/small molecules, cannot accommodate large protein molecules (~tens of nm in size). The surface area accessible by proteins (defined here as effective surface area, S_{EFF}) strongly depends on the pore diameter, D_p, of porous LDHs. To date, LDHs of micron- and submicron scale structures have been reported as particles,[10-11] sheets,[12] plates with grooves,[13] however, increasing S_{EFF} is challenging and hard to achieve with these materials. This is because LDH crystals as building-blocks used to assemble materials are relatively large, typically in sub-μm.[13-14] Limiting the dimensions of LDH crystals to nanoscale,

assembling them into 3D porous solids, and optimizing their meso and macroporous structures remains a big challenge when attempting to maximize S_{EFF} and thereby protein loading. Recently, we have reported the preparation of monolithic LDHs with hierarchical pores.[15] The hierarchical pores of macro (1 μm) and meso (8 nm) formed spontaneously via a facile sol-gel reaction. It was also reported that target oxyanions (CrO_4^{2-}, SO_4^{2-}, MoO_4^{2-}, etc) and small molecules diffuse rapidly through the macropores and adsorb on a large surface derived from the mesopores.[16] However, the development of LDHs with tens-nm-pores which are optimized to maximize S_{EFF} through structural hierarchy is still needed in order to exploit the applications of biocompatible solid supports with a high capacity for protein loading.

We here prepare biocompatible composites of LDH and aluminum hydroxide (Alhy) with two levels of hierarchical tunable pores in the range of tens-nm and a few-μm. Dependence of the mean mesopore diameter D_{pm} on the synthesis parameters were investigated to tune the hierarchical porosity of the LDH-Alhy. Then, the adsorption of a large protein, bovine serum albumin (BSA) on the LDH-Alhy surfaces of various S_{EFF} was conducted to establish a relationship between S_{EFF} and loading capacity (Fig. 1a). D_{pm} could be tuned from 12 nm to 53 nm, leading to a range of S_{EFF} for adsorption of BSA molecules. Particular interest was focused on aerogels obtained via supercritical drying[17-18] on which considerable adsorption of the large protein molecules were achieved owing to the maximized S_{EFF}. Finally, the capability of the LDH-Alhy to release the immobilized protein in HPO_4^{2-} and Cl^- aq. solutions was investigated (Fig. 1b). The encapsulation as well as the release of BSA was attempted by inducing the shrinkage of porous matrix after BSA loading (Fig. 1c). The results demonstrated here provide key quantitative insights into protein loading on hydroxide-based biocompatible materials that display 14 times higher loading capacity than referential LDH materials.

Experimental

3

Chemical. Aluminum chloride hexahydrate ($AlCl_3 \cdot 6H_2O$; 98%) and magnesium chloride hexahydrate ($MgCl_2 \cdot 6H_2O$; 98%) were used as inorganic sources. A mixture of ultrapure water and ethanol (EtOH; 99.5%) was used as a solvent. ($\pm$)-Propylene oxide (PO; >99%) and isopropyl alcohol (IPA; 99.7%) were employed as a proton scavenger and a liquid for sample washing, respectively. Poly(ethylene oxide) (PEO; $Mv = 1 \times 10^6$) was used as an organic additive. Dipotassium hydrogen phosphate (K_2HPO_4; >99%) and sodium chloride (NaCl; >99%), hydrochloric acid (HCl; 36.0 wt%) were used to trigger desorption of BSA. PO, PEO, and BSA were purchased from Sigma-Aldrich Co. and all other reagents were from Wako Pure Chemicals Industries, Ltd. All chemicals were used as received. For comparison, reference LDH (Ref-LDH) was prepared by a standard pH constant coprecipitation approach[19] with a chemical composition of $[Mg_{0.68}Al_{0.32}(OH)_2Cl_{0.21}(CO_3^{2-})_{0.06} \cdot yH_2O]$. A commercial LDH (Com-LDH $Mg_{0.75}Al_{0.25}(OH)_2(CO_3)_{0.125} \cdot 4H_2O$, Wako Pure Chemicals Industries, Ltd) was purchased and used for the further comparison.

Preparation of LDH-Alhy xerogels and aerogels. Typically, $AlCl_3 \cdot 6H_2O$ (1.58 g; 6.55 mmol), $MgCl_2 \cdot 6H_2O$ (1.06 g; 5.23 mmol), and various amount (W_{PEO}) g of PEO were dissolved in a mixture of water/ethanol (4.00 mL/3.00 mL). PO (1.82 mL; 26.2 mmol) was added to this solution maintained at 25 °C and stirred for 1 min to yield a homogenous sol. The sol was transferred to a polystyrene container, sealed, and kept at 40 °C. After 24 h, an opaque gel thus obtained was soaked in IPA for 1 h to exchange the water/EtOH solvent remained inside pores with IPA. This process was repeated at least 8 times with fresh IPA. Then, the gel was solvothermally treated in IPA at 180 °C for 24 h, followed by either ambient or supercritical drying. The ambient drying was performed at 40 and 120 °C in an oven to yield xerogels, named as "X-LDH-40" and "X-LDH-120", respectively. Supercritical drying was conducted with supercritical CO_2 (80 °C and 14.0 MPa), yielding aerogels which are labeled as "A-LDH" in this following.

Structural characterization. Fine structures of the samples were observed by a field emission scanning electron microscope (FE-SEM; S-4800, Hitachi, Japan). Crystal phases of the obtained samples were identified by X-ray diffraction (XRD; MultiFlex, Rigaku, Japan) using CuKα radiation ($\lambda = 0.154$ nm).

Micro–mesoporous characters of the samples were investigated by a N_2 adsorption–desorption apparatus (BELSORP-mini II, Bel Japan Inc., Japan). Prior to the measurement, the samples (A-LDH, X-LDH, Com-LDH, and Ref-LDH) were subjected to quick heat treatment to remove water adsorbed (500 °C), and then further outgassed under vacuum at 200 °C. The pore size distribution was calculated from the adsorption branch of the isotherm by the Barrett–Joyner‑Halenda (BJH) method. Mean pore diameter, D_{pm}, and total pore volume, V_p (integrated pore volume in the range of $D_p < 183$ nm) were estimated from the distribution curves. The BJH method was also applied to assess partial specific surface area ($S_{(>xnm)}$) derived from pores larger than a cut-off value. For example, $S_{(>5nm)}$ corresponds to a specific surface area obtained by integrating surfaces of pores of $D_P > 5$ nm. The Brunauer–Emmett–Teller (BET) method was also applied to estimate specific surface area, S_{BET}. Synchrotron X-ray micro-computed tomography (μ-CT) was employed to non-destructively obtain three dimensional (3D) images of the drying process of the monoliths. High resolution synchrotron-based X-ray tomographic image was obtained from the Diamond-Manchester branchline I13-2 at Diamond Light Source.[20] The samples were kept at 300 K on the beamline using an in house environmental stage.[21] A polychromatic filtered parallel-beam setup was used with a 0.81 μm effective pixel size and ~2 μm spatial resolution. Over the 180° rotation, 3600 projections were collected at 0.05 s exposure time and tomographically reconstructed into a 3D volume using software developed at Diamond Light Source.[22] Visualisation package Avizo® was used to produce the 3D images and quantify shrinkage. The gel samples for the μ-CT measurements were prepared from $AlCl_3 \cdot 6H_2O$ (2.19 g), $MgCl_2 \cdot 6H_2O$ (0.553 g), $W_{PEO} = 0.03$ g, water (4.00 mL), ethanol (3.00 mL), and PO (2.27mL).

BSA sorption test. Each of LDH xerogels (25 mg/mL), LDH aerogels (1.5 mg/mL), Ref-LDH (7.5 mg/mL), and Com-LDH (10 mg/mL; $Mg_6Al_2(OH)_{16}CO_3 \cdot 4H_2O$, Wako Pure Chemicals Industries, Ltd) was dispersed in aqueous BSA solutions of various concentrations (1.0-3.5 mg/mL) (Supporting note is in SI). The mixtures were placed at 25 °C for 72 h. Supernatants of respective mixtures were collected through a membrane filter (0.45 μm), and analyzed by ultraviolet-visible spectroscopy (UV-Vis: V-670

5

spectrophotomater, JASCO Corp.) The concentration of BSA was estimated by Beer-Lambert law using peak intensity at 277.4 nm. The amount of adsorbed BSA was calculated from equation (1),

$$C_s = \frac{(C_i - C_{eq}) \times V}{m} \qquad (1)$$

, where C_s (mg/g) is the amount of BSA adsorbed by LDH, C_i (mg/mL) and C_{eq} (mg/mL) are initial and equilibrium concentrations of BSA in the solution, V (mL) is the volume of the solution, and m (g) is the mass of LDH. Freundlich equation (eq. (2)) was used as isotherm model for BSA adsorption on the alumina-LDH composites.

$$log\, C_s = \, logK_f + \frac{1}{n_f}\, logC_{eq} \qquad (2)$$

, where K_f (mg/g) is Freundlich constant and n_f is the adsorption intensity. The BSA adsorption tests were conducted on LDH-Alhy composites prepared at $W_{PEO} = 0, 0.01, 0.02, 0.03, 0.04$. To study BSA desorption, 30 mg of the sample which had previously adsorbed BSA in the solution of BSA concentration of 2.5 mg/mL (25 °C for 72 h) was immersed in 0.1 M NaCl and 0.1 M K_2HPO_4 aq (25 °C for 72 h), respectively. The amounts of BSA molecules desorbed from the A-LDH (W_{PEO}=0.02 g) and Com-LDH were analyzed by the UV-Vis technique. Some of A-LDHs were dried after BSA adsorption (before desorption test) and the effect of shrinkage on desorption was investigated. The reproducibility of adsorption isotherms were assessed on Com-LDH and X-LDH-40 (details in Supplementary Information).

Results and Discussion

Synthesis of hierarchically porous LDH-Alhy with tunable porosities

The hierarchically porous LDH-Alhy composites were prepared via hydrolysis and condensation reactions of metal salts by alkalinization in the presence of propylene oxide (PO) according our previously published method.[15] PO is a proton scavenger which increases pH of the solution[23] to precipitate LDHs. This reaction process yields nano-sized hydroxide particles (crystals) and leads to

6

homogenous gelation in 15 min, due to a high degree of supersaturation generated in the reaction solution. The gelling solution phase-separates [24-25] into LDH-Alhy-rich solid phase and PEO-rich fluid phase. Evaporative removal of the fluid phase leaves macropores (in μm range). Simultaneously, the mesopores (in nm range) were formed within the gel skeleton (Fig. 1a). The mesopore size, D_p, and mesopores volume, V_p, which expectedly influence the S_{EFF} and the adsorption capacity of LDHs, varied as a function of W_{PEO} (the amount of PEO additive) and drying conditions.

Figure 2 shows XRD patterns and SEM images of the different LDH-Alhy composites and Ref-LDH. The composites and Ref-LDH are ascribed to hydrotalcite-type LDH with typical PXRD patterns of a R-3m hexagonal lattice.[26] Crystallite sizes estimated from Scherrer's equation using the (003) diffraction peak are 24 nm for Ref-LDH, 7.2 nm for X-LDH-40, 7.1 nm for X-LDH-120, and 6.8 nm for A-LDH. These values evidence that the crystallite sizes of X-LDH and A-LDH are comparable and far smaller than Ref-LDH used here as the reference, considered as a poorly crystallized material. Chemical analysis revealed that the LDH-Alhy composites have the composition of $[Mg_{0.66}Al_{0.33}(OH)_2Cl_{0.33-x}(CO_3^{2-})_{x/2} \cdot yH_2O] \cdot 2.0Al(OH)_3$. Alhy which forms porous networks together with LDH crystals display hydroxylated surface that are biocompatible with proteins, as confirmed by their use as adjuvant in some vaccines.[27] As a result, the LDH-Alhy composites offer extensive solid surface used for protein loading.

The LDH-Alhy composites produced here and Ref-LDH possess very different microstructures (Fig. 2). The morphology of Ref-LDH is aggregates of LDH plates with the size of 1-4 μm. On the other hand, LDH-Alhy composites possess hierarchically porous structures with a monolithic form. As well as interconnected macropores with the pore diameter of a few μm, mesopores are confirmed in the gel skeletons (higher magnification images in Fig. 2). The difference of mesostructures is clearly supported by N_2 sorption measurements (Table 1). Large BET surface areas exceeding 400 m^2/g are derived from the mesoporosity which are formed as interstices of constituent nanoparticles. The BJH pore size distributions of Ref-LDH, Com-LDH, and LDH-Alhy composites are plotted in Figs. S1 and S2. Com-LDH and Ref-LDH have negligible mesopores, whereas LDH-Alhy composites possess considerable

pore volume of 0.94-4.27 cm^3/g, originated from pores in the range of $D_p < 150$ nm. PEO changes the assembly of LDH and Alhy particles, and D_{pm} decreases with increasing W_{PEO} (Table 1). The formation of smaller mesopores with increasing W_{PEO} is caused by increased phase contrast leading to a more packed LDH and Alhy crystallites.[18, 28] The characteristics of mesopores also depends on the drying conditions. A-LDHs possess the largest D_{pm} and V_p among the three sets of LDH-Alhy composites because the shrinkage is minimized by applying the supercritical drying.[17] To get better insight on the shrinkage upon drying process of the monolithic LDHs, X-ray μ-CT was performed while the gels were left to dry at 300 K (Fig. 3). Figure 3 shows 3D images of a small volume of the same gel before and after drying. It shows that shrinkage was isotropic, leading to a volume shrinkage of 85% and a linear shrinkage of 46%. The relatively large D_{pm} and V_p of X-LDH-120 compared to X-LDH-40 is due to smaller degree of shrinkage on drying. The faster drying at 120 °C forms cracks in the monolithic specimen and releases stress generated at the drying front, retarding isotropic shrinkage and leading to larger mesopores.[29] It should be emphasized again that X-LDH-40, X-LDH-120, and A-LDHs possess the identical chemical composition and the crystallinity, and differences among these samples are only porosity in nm and μm scales. In summary, D_{pm} of LDH-Alhy composites were successfully tuned between 12 nm and 53 nm by W_{PEO} value and drying condition.

Effect of pore structure on protein adsorption

The LDH-Alhy composites with various D_{pm} and V_p were assessed as bio-supports with a high capacity for protein loading. As an adsorbate, BSA was used, which is a large multi-domain protein with a hydrodynamic radius of 3.6 nm and 3D size of 5×7×7 nm^3.[30] Serum albumin, a major soluble constituent of the plasma proteins, has many physiological functions.[31] Moreover, BSA has been used as a model protein to investigate reactions of physiological disorders, such as diabetes,[32] and its sustained-release[33], immobilization[7], and bio-probes are of interest.[34] Aluminum hydroxide and LDH, have been individually used in the crystalline platelet to form as adsorbents for BSA molecules.[35-37] Preliminary results (not shown) of BSA adsorption using previously-reported hierarchically porous LDHs[15]

(prepared by ambient drying without the solvothermal treatment) lead to negligible amount of protein adsorption. Where, mesopore size was too small to accommodate protein molecules, and only macropores were available for protein adsorption; surface area derived from macropores[38] is less than 10 m^2/g.

Figure 4a represents adsorption isotherms of BSA on X-LDH-40 at different W_{PEO}. At W_{PEO} =0, 0.01, and 0.02 g, the adsorption of BSA was negligible. LDH-Alhy composites prepared at W_{PEO} =0 g and 0.01 g do not possess any macropores, limiting BSA adsorption to the external surface where BSA adsorbed on the surface prevents further diffusion of protein through the mesopores into the bulk of the material. On the other hand, LDH-Alhy with hierarchically porous structure (W_{PEO} =0.03-0.04 g and macropores of 1 μm) show much higher BSA loading due to the presence of co-continuous macropores channels for BSA molecules to diffuse through to majority of the available surface. Corresponding adsorption isotherms of X-LDH-120 and A-LDH are plotted in Fig. 4b and c, respectively. Due to the lack of realistic adsorption models for fitting the interactions between solid surfaces and proteins, many studies have reported the use of Freundlich model as an approximative tool to evaluate and compare various solid/protein systems.[39] Freundlich adsorption isotherms for X-LDH-40, X-LDH-120, and A-LDH are represented in Fig. S3. The plots can be linearly fitted by equation (2) except for the case of X-LDH-40 at W_{PEO} =0.02 g whose microstructure is highly inhomogeneous because of structure deformation during drying. K_f value increases in the order of X-LDH-40 < X-LDH-120 < A-LDH as summarized in Table 2. The Freundlich constant, K_f, of A-LDH prepared with W_{PEO} =0.02 g is 996 mg·g^{-1}. The value is 14 times that of Ref-LDH (70 mg·g^{-1}), confirming that A-LDH composites prepared in the present study exhibit excellent adsorption properties compared to X-LDH and Ref-LDH. Clearly, the porous structure is the key factor that accounts for BSA loading while different influences, slight pH change during adsorption and difference of hydroxylated surfaces, are negligible (Tables S1 and S2). Indeed, while surface of Ref-LDH with a higher zeta potential (42 mV) should promote higher BSA adsorption than LDH/Alhy composite (37 mV for X-LDH-40), the reverse is observed; BSA has an isoelectric point of pI = 4.7[40] and is negatively-charged in the present adsorption condition (pH= ~7).

Figure 5 shows a plot of K_f values of LDH-Alhy composites against $S_{(>x\text{nm})}$. $S_{(>x\text{nm})}$ is a specific surface area obtained by integrating surface areas derived from pores of $D_p > x$ nm; for example, $S_{(>5\text{nm})}$ is a sum of surface areas derived from pores with a diameter of $D_p > 5$ nm. The LDH-Alhy composites prepared in the present study have tunable pore characteristics and $S_{(>x\text{nm})}$ was controllable to a large extent. Figure 5 shows K_f values against $S_{(>x\text{nm})}$ for $x = 5$, 10, 15, and 20 nm pore size. K_f and $S_{(>5\text{nm})}$ do not have correlation because relatively small mesopores cannot accommodate BSA. The surface area, which is derived from the mesopores whose sizes are insufficient for BSA adsorption, less contributes to $S_{(>x\text{nm})}$ as x value becomes larger. As a result, linear least square fitting gives better correlation coefficient r with increasing x. At $x = 15$ nm and 20 nm, r was estimated as 0.77 and 0.92, respectively. These results reveal that D_p of ca. 20 nm is the threshold which allows to accommodate and adsorb BSA molecules on the entire surfaces of mesopores. Although the pores of 10-20 nm is apparently larger than the size of BSA molecules ($5\times7\times7$ nm^3), adsorption on the surface of these relatively small mesopores does not take place efficiently because entrance of mesopores is blocked by the first few BSA molecules adsorbing there. This effect was indeed observed for X-LDH-40 ($W_{\text{PEO}} = 0\text{-}0.02$), in which mesopores ($D_{\text{pm}} < 15$ nm) in the absence of macropores exhibited negligible adsorption (Fig. 4a). Similar size effect of mesopores on BSA adsorption was qualitatively reported on mesoporous silica, where SBA-15 with the pore diameter of 24 nm showed much better BSA adsorption than those with 3.8 and 7.7 nm in diameters.[41] The present results give a very systematic and quantitative evidence for a threshold in pore diameter for effective adsorption of BSA molecules to mesoporous materials. The approach demonstrated here will be a promising platform to maximize S_{EFF} for respective proteins with different molecular sizes.

Ability for encapsulation and releasing of immobilized proteins

The capability of encapsulating immobilized protein and their sustained-release are also important feature for bio-adsorbents. A previous study reported that BSA desorption from Zn-Al LDH took place by the addition of competitive anionic adsorbates.[42] Herein, HPO_4^{2-} and Cl^- ions were used as

competitive ions to release pre-adsorbed BSA molecules. Table 3 summarizes the results of protein desorption from A-LDH and Com-LDH. 52% of BSA desorbed in 72 h from A-LDH in the case of using HPO_4^{2-} as competitive anion, which is comparable to that from the Com-LDH (49%). This result confirms that the protein desorption as well as the adsorption takes place with a large capacity for the present LDH-Alhy composites. Whereas, in the case of using Cl^- solution for desorption, BSA adsorption was retained for both Com-LDH and A-LDH, which is due to the lower affinity of Cl^- and LDH surface, and smaller minus charge compared to HPO_4^{2-}. Whereas the LDH-Alhy composites (X-LDH and A-LDH) have a weight ratio of LDH : Alhy = 1 : 1, the desorption percentage by Cl^- of these composites is almost same as pure LDH (~2%) (Table 3). A simple integration of respective surfaces of LDH and $Al(OH)_3$ cannot explain the low BSA desorption from A-LDH composite observed with Cl^- as the counter ion because BSA desorption easily occurs on Alhy (50-60%) by using Cl^- as a competitive ion. The unique surface texture of A-LDH, the nanomosaic surface composed of Alhy and LDH nanoparticles, would result in the peculiar restricted desorption, though further evidence is required. BSA molecules were also entrapped in the matrix of the composite by first immobilizing BSA within A-LDH which was then dried to trap the protein within as the gel shrunk. As summarized in Table 3 and Fig. 6, the desorption of BSA molecules by HPO_4^{2-} from dried samples was <23%, which is less than half that of the non-dried sample of its original dimension (52%). These results demonstrate the possibilities of encapsulation and extended-release of various protein molecules with a high capacity based on tunable hierarchically porous LDH. Combining LDH materials with various selectivities towards different molecules/ions will further open up biocompatible separation and purification required for biomedical applications.[43]

Conclusions

The successful preparation of biocompatible LDH-Alhy composites with an optimized S_{EFF} for large protein molecules is presented. S_{EFF} could be altered by the synthesis parameters, such as the amount of polymer additive and the drying conditions used. Capacity for protein loading was investigated with

BSA as the model protein, which revealed the existence of a threshold on lower critical mesopore size required to accommodate BSA molecules to be ca. $D_P = 20$ nm. Especially, the LDH-Alhy aerogel (W_{PEO} =0.02 g) with a hierarchically porous structure and median mesopore size of 53.2 nm exhibited a remarkably high protein loading ($K_f = 996$ mg·g^{-1}) when compared to Ref-LDH and Com-LDH standards. The BSA molecules pre-adsorbed on the composite were released by HPO_4^{2-} as a competitive adsorbate. While, when Cl^- was the competing ion, BSA release was retarded to the extent comparable to pure LDH; presumably because of the unique surface texture, nanomosaic of LDH and $Al(OH)_3$. The tunable mesostructures in the range of nm to tens of nm are applicable to molecular sieving and purification of protein solutions. Further investigation based on this platform would open up many possibilities of using these hierarchically porous LDH-Alhy composites in various applications.
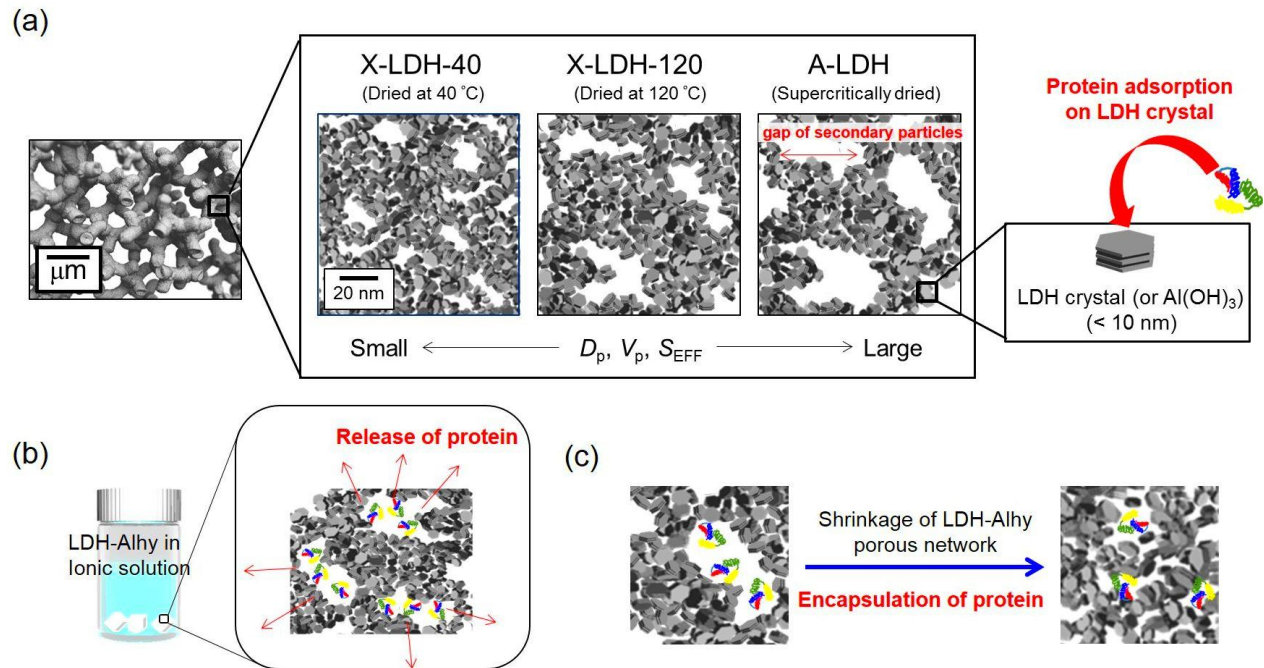
Figure 1. Schematic illustration depicting the research carried out in this study. (a) LDH nanocrystals and Alhy nanoparticles form biocompatible solids with hierarchically porous structures. (b) The pre-adsorbed proteins (BSA) released by soaking the composite in solutions containing competitive anionic adsorbates (HPO_4^{2-} and Cl^-). (c) Large shrinkage of mesoporous networks (length shrinkage of 50 %) upon drying leading to successfully-encapsulated BSA molecules.
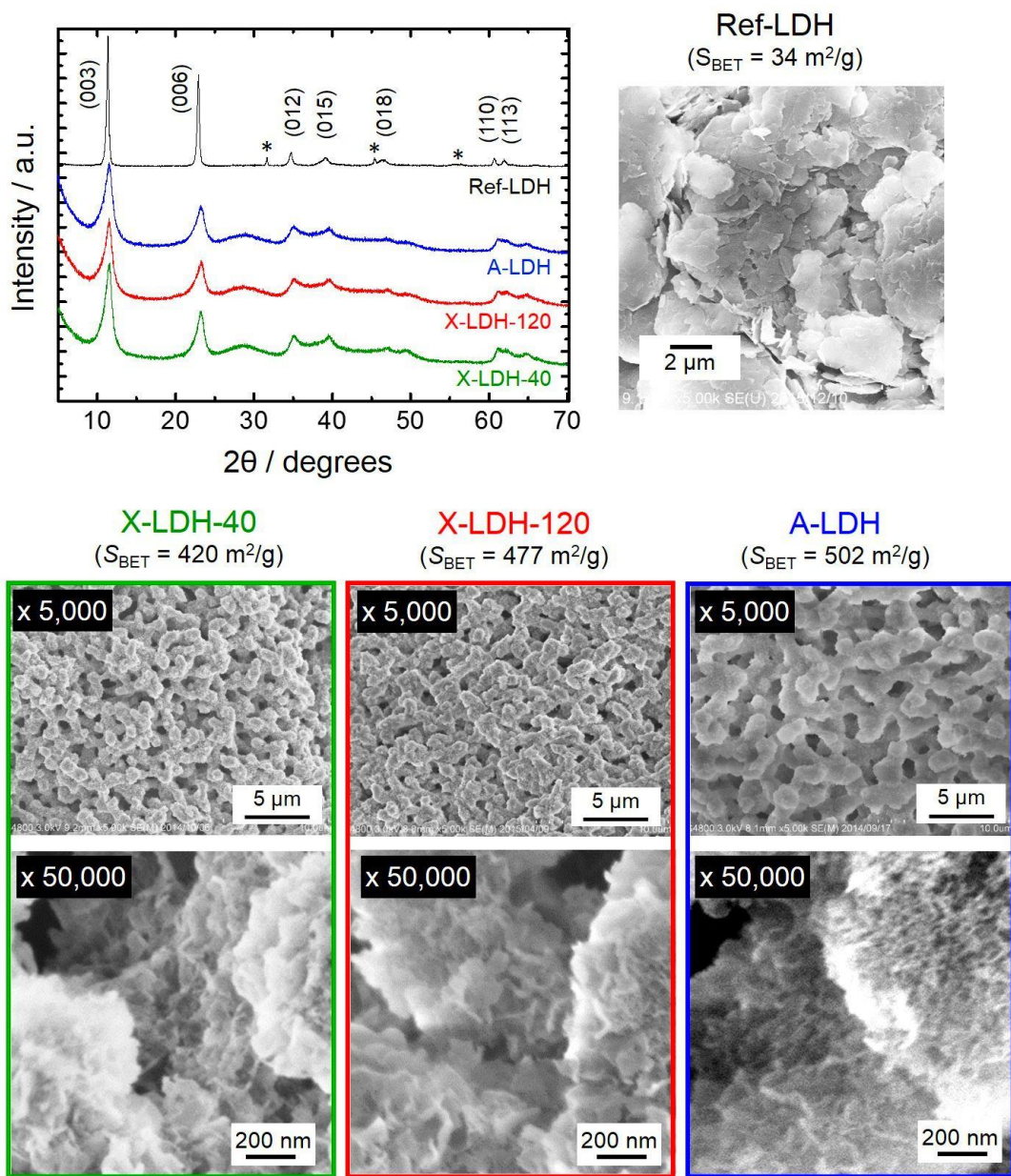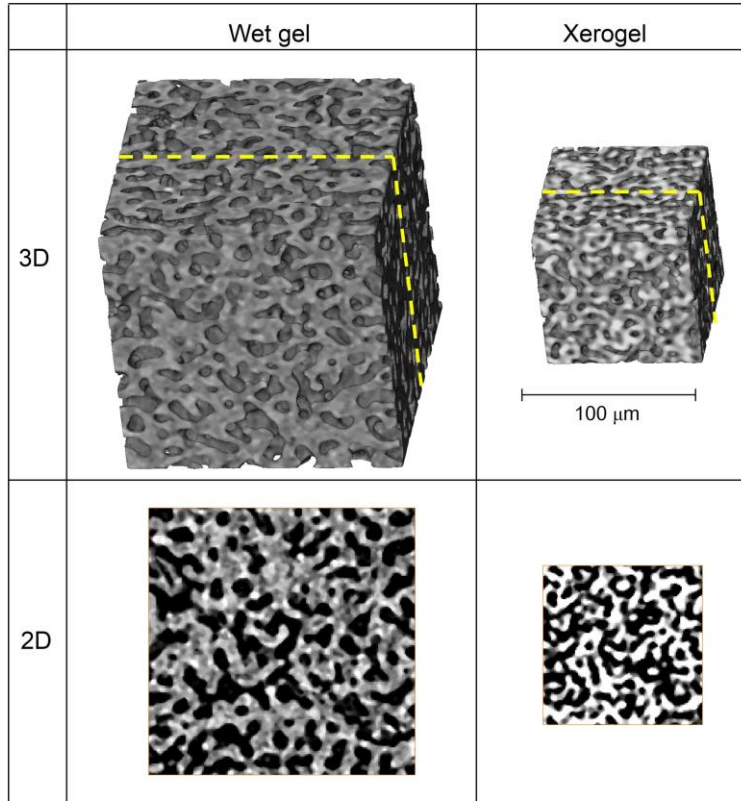
Figure 2. XRD patterns and FE-SEM images of Ref-LDH, X-LDH-40, X-LDH-120, and A-LDH. (Hydrotalcite JCPDS# 00-022-0700). W_{PEO} = 0.03 g. *: impurity NaCl phase.

	Wet gel	Xerogel
Solid fraction (%)	57	61
Pore fraction (%)	43	39
Length Shrinkage (%)	N/A	46
Volume Shrinkage (%)	N/A	85

Figure 3. 3D and 2D X-ray micro-computed tomography (μ-CT) images of the LDH-Alhy composites before (wet gel) and after (xerogel) drying at 300 K. The wet gel sample for μ-CT was prepared at Mg/Al = 0.3 and W_{PEO}=0.03 g. Isotropic shrinkage took place during the drying, leading to the volume shrinkage of 85% and the linear shrinkage of 46%. Images were reconstructed from the same part of the monolithic sample. The yellow dotted lines in 3D images represent 2D planes shown as 2D images.
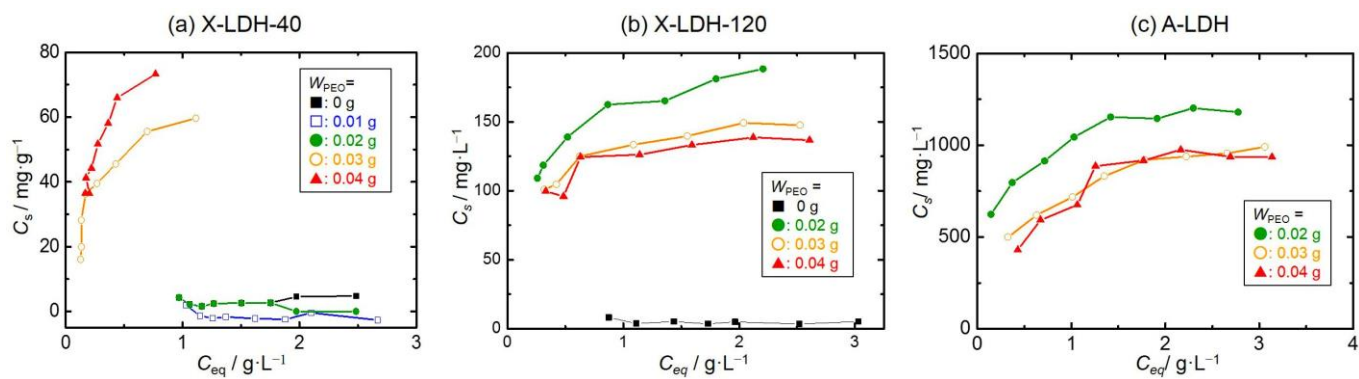
Figure 4. BSA adsorption isotherms on (a) X-LDH-40, (b) X-LDH-120, (c) A-LDH at 25 °C. Adsorption isotherms of BSA on A-LDH prepared at W_{PEO}= 0 and 0.01 g (without macropores) are not reproducible.

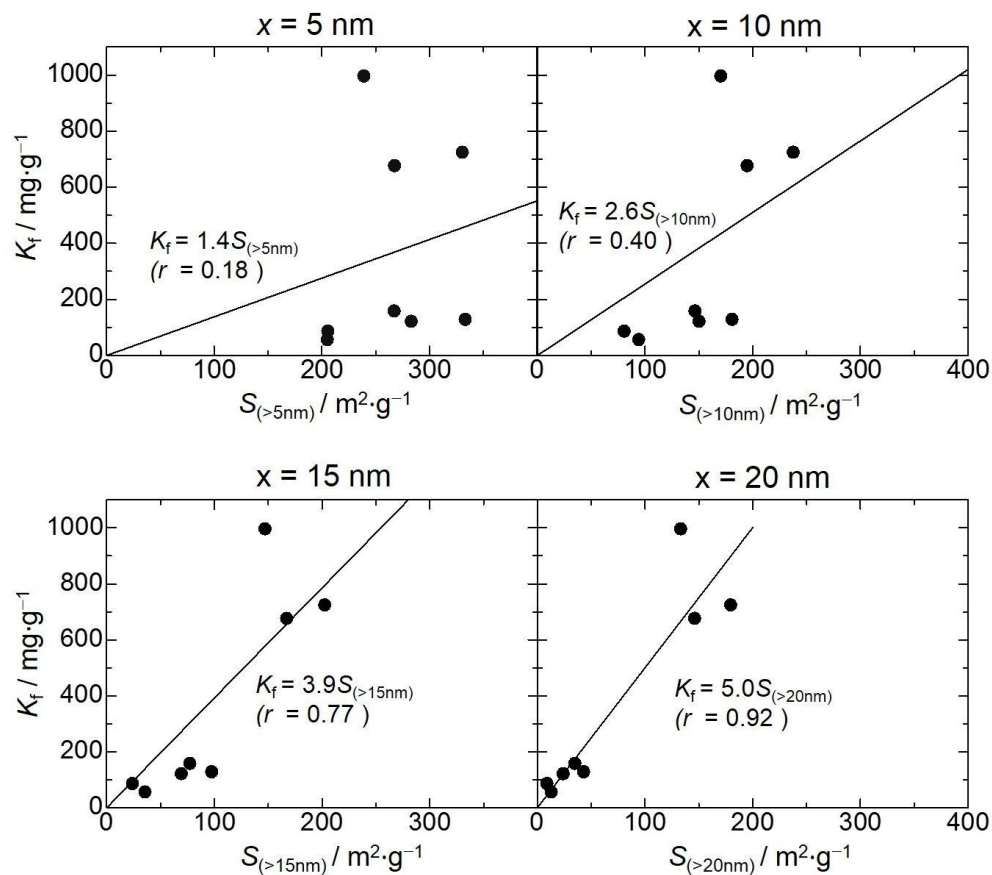**Figure 5.** K_f vs $S_{(>xnm)}$ of LDH-Alhy composites. K_f values listed of LDH-Alhy composites listed in Table 2 are plotted. $S_{(>xnm)}$: specific surface areas derived from the pores larger than x nm. The results of linear least square fitting are depicted with the plots. r: correlation coefficient.
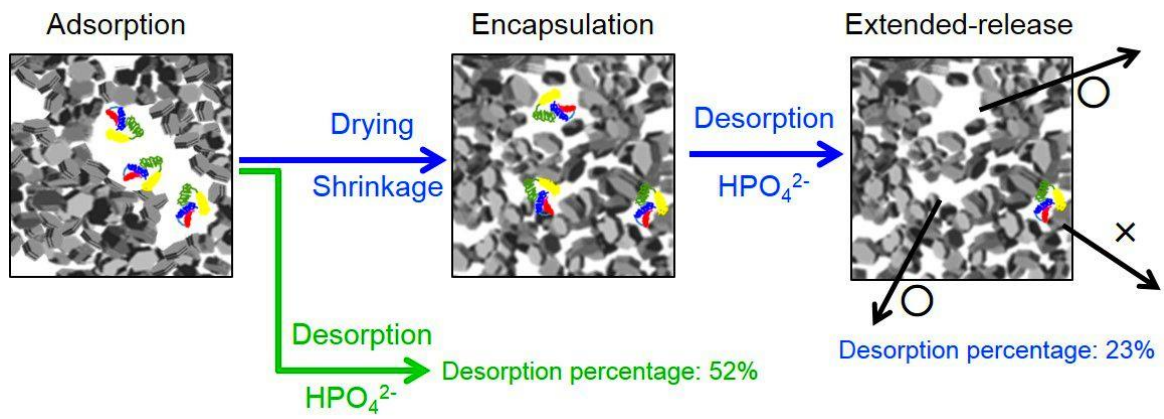
Figure 6. Schematic illustration showing the controllable release of BSA adsorbed on A-LDH.

Table 1. Mesopore characteristics of LDH-Alhy composites.

	X-LDH-40			X-LDH-120			A-LDH			Ref-LDH	Com-LDH
W_{PEO} /g	0.02	0.03	0.04	0.02	0.03	0.04	0.02	0.03	0.04	−	−
D_{pm} / nm	14.1	14.1	12.3	19.9	16.9	15.5	53.2	40.8	38.1	−	−
V_p /cm^{3}g^{-1}	0.94	1.04	0.95	1.44	1.70	1.40	3.82	4.27	3.15	−	−
S_{BET} /m^{2}g^{-1}	390	420	389	394	477	397	397	502	380	34	123
$S_{(>2nm)}$ /m^{2}g^{-1}	357	343	351	418	521	439	359	491	391	40	77

Table 2. Summary of Freundlich fitting of BSA on solid surfaces.

Entry	W_{PEO}	K_f (mg·g^{-1})	$1/n_f$	R^2
Ref-LDH	−	70	0.32	0.93
Com-LDH	−	138	0.23	0.97
X-LDH-40	0.02	NA	NA	NA
	0.03	56	0.28	0.97
	0.04	86	0.41	0.95
X-LDH-120	0.02	158	0.24	0.96
	0.03	128	0.19	0.94
	0.04	121	0.17	0.78
A-LDH	0.02	996	0.23	0.97
	0.03	724	0.32	0.98
	0.04	676	0.40	0.85

Table 3. Capability of controllable release of BSA from the LDH-Alhy composite. *BSA adsorbed A-LDH was dried and immersed in aqueous solution of releasing agent, HPO_4^{2-}.

Entry	Releasing agent	Releasing percentage (%)
Com-LDH	HPO_4^{2-}	49
	Cl^-	1.1
A-LDH	HPO_4^{2-}	52
	Cl^-	1.8
	HPO_4^{2-*}	23

References and Notes

1.   Mansur, H. S.; Lobato, Z. P.; Oréfice, R. L.; Vasconcelos, W. L.; Oliveira, C.; Machado, L. J., Surface functionalization of porous glass networks: Effects on bovine serum albumin and porcine insulin immobilization. *Biomacromolecules* **2000,** *1* (4), 789-797.

2.   Yuan, S. J.; Wan, D.; Liang, B.; Pehkonen, S. O.; Ting, Y. P.; Neoh, K. G.; Kang, E. T., Lysozyme-Coupled Poly(poly(ethylene glycol) methacrylate)-Stainless Steel Hybrids and Their Antifouling and Antibacterial Surfaces. *Langmuir* **2011,** *27* (6), 2761-2774.

3.   Zhu, L. P.; Jiang, J. H.; Zhu, B. K.; Xu, Y. Y., Immobilization of bovine serum albumin onto porous polyethylene membranes using strongly attached polydopamine as a spacer. *Colloid Surface B* **2011,** *86* (1), 111-118.

4.   Guérard-Hélaine, C.; Légeret, B.; Fernandes, C.; Prévot, V.; Forano, C.; Lemaire, M., Efficient immobilization of fructose-6-phosphate aldolase in layered double hydroxide: Improved stereoselective synthesis of sugar analogues. *New J. Chem.* **2011,** *35* (4), 776-779.

5.   An, Z.; Lu, S.; He, J.; Wang, Y., Colloidal Assembly of Proteins with Delaminated Lamellas of Layered Metal Hydroxide. *Langmuir* **2009,** *25* (18), 10704-10710.

6.   Mandal, H. S.; Kraatz, H. B., Effect of the surface curvature on the secondary structure of peptides adsorbed on nanoparticles. *J. Am. Chem. Soc.* **2007,** *129* (20), 6356-+.

7.   Roach, P.; Farrar, D.; Perry, C. C., Surface tailoring for controlled protein adsorption: Effect of topography at the nanometer scale and chemistry. *J. Am. Chem. Soc.* **2006,** *128* (12), 3939-3945.

8.   Charradi, K.; Forano, C.; Prevot, V.; Madern, D.; Amara, A. B. H.; Mousty, C., Characterization of hemoglobin immobilized in MgAl-layered double hydroxides by the coprecipitation method. *Langmuir* **2010,** *26* (12), 9997-10004.

9.   Li, M.; Ji, H.; Wang, Y.; Liu, L.; Gao, F., MgFe-layered double hydroxide modified electrodes for direct electron transfer of heme proteins. *Biosens. Bioelectron.* **2012,** *38* (1), 239-244.

10.   Touisni, N.; Charmantray, F.; Helaine, V.; Forano, C.; Hecquet, L.; Mousty, C., Optimized immobilization of transketolase from E. coli in MgAl-layered double hydroxides. *Colloids and Surfaces B: Biointerfaces* **2013,** *112*, 452-459.

11.   Shao, M.; Ning, F.; Zhao, J.; Wei, M.; Evans, D. G.; Duan, X., Preparation of Fe 3O 4@SiO 2@layered double hydroxide core-shell microspheres for magnetic separation of proteins. *J. Am. Chem. Soc.* **2012,** *134* (2), 1071-1077.

12.   Wang, Q.; O'Hare, D., Recent Advances in the Synthesis and Application of Layered Double Hydroxide (LDH) Nanosheets. *Chem. Rev.* **2012,** *112* (7), 4124-4155.

13.   Guo, X. X.; Zhang, F. Z.; Evans, D. G.; Duan, X., Layered double hydroxide films: synthesis, properties and applications. *Chem. Commun.* **2010,** *46* (29), 5197-5210.

14.   Ni, X. M.; Kuang, K. Q.; Jin, X.; Xiao, X. K.; Liao, G. X., Large scale synthesis of porous microspheres of Mg-Al-layerd double hydroxide with improved fire suppression effectiveness. *Solid State Sci* **2010,** *12* (4), 546-551.

15.   Tokudome, Y.; Tarutani, N.; Nakanishi, K.; Takahashi, M., Layered double hydroxide (LDH)-based monolith with interconnected hierarchical channels: enhanced sorption affinity for anionic species. *Journal of Materials Chemistry A* **2013,** *1* (26), 7702-7708.

16.   Tarutani, N.; Tokudome, Y.; Nakanishi, K.; Takahashi, M., Layered double hydroxide composite monoliths with three-dimensional hierarchical channels: structural control and adsorption behavior. *Rsc Adv* **2014,** *4* (31), 16075-16080.

17.   Touati, S.; Mansouri, H.; Bengueddach, A.; de Roy, A.; Forano, C.; Prevot, V., Nanostructured layered double hydroxide aerogels with enhanced adsorption properties. *Chem. Commun.* **2012,** *48* (57), 7197-7199.

18.   Tokudome, Y.; Nakanishi, K.; Kanamori, K.; Fujita, K.; Akamatsu, H.; Hanada, T., Structural characterization of hierarchically porous alumina aerogel and xerogel monoliths. *J. Colloid Interface Sci.* **2009,** *338* (2), 506-513.

19.   Inacio, J.; Taviot-Gueho, C.; Forano, C.; Besse, J. P., Adsorption of MCPA pesticide by MgAl-layered double hydroxides. *Appl Clay Sci* **2001,** *18* (5-6), 255-264.

20.   Rau, C.; Wagner, U.; Pesic, Z.; De Fanis, A., Coherent imaging at the Diamond beamline I13. *Physica Status Solidi a-Applications and Materials Science* **2011,** *208* (11), 2522-2525.

21.   Rockett, P.; Karagadde, S.; Guo, E.; Bent, J.; Hazekamp, J.; Kingsley, M.; Vila-Comamala, J.; Lee, P. D. In *A 4-D dataset for validation of crystal growth in a complex three-phase material, ice cream*, IOP Conference Series: Materials Science and Engineering, **2015.**

22.   Atwood, R. C.; Bodey, A. J.; Price, S. W. T.; Basham, M.; Drakopoulos, M., A high-throughput system for high-quality tomographic reconstruction of large datasets at Diamond Light Source. *Philos T R Soc A* **2015,** *373* (2043).

23.   Gash, A. E.; Tillotson, T. M.; Satcher, J. H.; Poco, J. F.; Hrubesh, L. W.; Simpson, R. L., Use of epoxides in the sol-gel synthesis of porous iron(III) oxide monoliths from Fe(III) salts. *Chem. Mater.* **2001,** *13* (3), 999-1007.

24.   Tokudome, Y.; Fujita, K.; Nakanishi, K.; Miura, K.; Hirao, K., Synthesis of monolithic Al2O3 with well-defined macropores and mesostructured skeletons via the sol-gel process accompanied by phase separation. *Chem. Mater.* **2007,** *19* (14), 3393-3398.

25.   Nakanishi, K., Pore Structure Control of Silica Gels Based on Phase Separation. *J. Porous Mater.* **1997,** *4* (2), 67-112.

26.   Roussel, H.; Briois, V.; Elkaim, E.; de Roy, A.; Besse, J. P., Cationic order and structure of [Zn-Cr-Cl] and [Cu-Cr-Cl] layered double hydroxides: A XRD and EXAPS study. *J. Phys. Chem. B* **2000,** *104* (25), 5915-5923.

27.   Kreuter, J., Nanoparticle-Based Drug Delivery Systems. *J. Controlled Release* **1991,** *16* (1-2), 169-176.

28.   Kanamori, K.; Kodera, Y.; Hayase, G.; Nakanishi, K.; Hanada, T., Transition from transparent aerogels to hierarchically porous monoliths in polymethylsilsesquioxane sol-gel system. *J. Colloid Interface Sci.* **2011,** *357* (2), 336-344.

29.   Brinker, C. J.; Scherer, G. W., Sol-Gel Science: The Physics and Chemistry of Sol-Gel Processing *Academic Press, San Diego, 1990.*

30.   Leggio, C.; Galantini, L.; Konarev, P. V.; Pavel, N. V., Urea-Induced Denaturation Process on Defatted Human Serum Albumin and in the Presence of Palmitic Acid. *J. Phys. Chem. B* **2009,** *113* (37), 12590-12602.

31.   He, X. M.; Carter, D. C., Atomic-Structure and Chemistry of Human Serum-Albumin. *Nature* **1992,** *358* (6383), 209-215.

32.   Reddy, S.; Bichler, J.; Wellsknecht, K. J.; Thorpe, S. R.; Baynes, J. W., N-Epsilon-(Carboxymethyl)Lysine Is a Dominant Advanced Glycation End-Product (Age) Antigen in Tissue Proteins. *Biochemistry-Us* **1995,** *34* (34), 10872-10878.

33.   Calvo, P.; RemunanLopez, C.; VilaJato, J. L.; Alonso, M. J., Novel hydrophilic chitosan-polyethylene oxide nanoparticles as protein carriers. *J. Appl. Polym. Sci.* **1997,** *63* (1), 125-132.

34.   Qin, W.; Ding, D.; Liu, J. Z.; Yuan, W. Z.; Hu, Y.; Liu, B.; Tang, B. Z., Biocompatible Nanoparticles with Aggregation-Induced Emission Characteristics as Far-Red/Near-Infrared Fluorescent Bioprobes for In Vitro and In Vivo Imaging Applications. *Adv. Funct. Mater.* **2012,** *22* (4), 771-779.

35.   Monash, P.; Majhi, A.; Pugazhenthi, G., Separation of bovine serum albumin (BSA) using gamma-Al2O3-clay composite ultrafiltration membrane. *J. Chem. Technol. Biotechnol.* **2010,** *85* (4), 545-554.

36.   Chao, V. W. K.; Hsu, C. C.; Lu, W. M.; Chen, W. J.; Naveen, B.; Tsai, T. Y., Protein-concentration-dependent adsorption behaviour of inorganic layered materials. *Rsc Adv* **2015,** *5* (15), 10936-10943.

37.   Gu, Z.; Zuo, H. L.; Li, L.; Wu, A. H.; Xu, Z. P., Pre-coating layered double hydroxide nanoparticles with albumin to improve colloidal stability and cellular uptake. *Journal of Materials Chemistry B* **2015,** *3* (16), 3331-3339.

38.   Tokudome, Y.; Nakanishi, K.; Kosaka, S.; Kariya, A.; Kaji, H.; Hanada, T., Synthesis of high-silica and low-silica zeolite monoliths with trimodal pores. *Microporous Mesoporous Mater.* **2010,** *132* (3), 538-542.

39.   Vanessa Prevot, C. M., Claude Forano (Editted by James C. Taylor), State of the Art in Biomolecule and Layered Double Hydroxide Assemblies *Advances in Chemistry Research, Volme 17, Nova Scientific Publishers* **2012**, 35-84.

40.   Chun, K. Y.; Stroeve, P., Protein transport in nanoporous membranes modified with self-assembled monolayers of functionalized thiols. *Langmuir* **2002,** *18* (12), 4653-4658.

41.   Katiyar, A.; Ji, L.; Smirniotis, P.; Pinto, N. G., Protein adsorption on the mesoporous molecular sieve silicate SBA-15: effects of pH and pore size. *J. Chromatogr. A* **2005,** *1069* (1), 119-126.

42.   Zhang, T.; Zhou, Y. M.; He, M.; Zhu, Y. X.; Bu, X. H.; Wang, Y. J., Biomimetic fabrication of hierarchically structured LDHs/ZnO composites for the separation of bovine serum albumin. *Chem. Eng. J.* **2013,** *219*, 278-285.

43.   Ma, W.; Lv, T. F.; Song, X. Y.; Cheng, Z. H.; Duan, S. B.; Xin, G.; Liu, F. J.; Pan, D. C., Characteristics of selective fluoride adsorption by biocarbon-Mg/Al layered double hydroxides composites from protein solutions: Kinetics and equilibrium isotherms study. *J. Hazard. Mater.* **2014,** *268*, 166-176.